JOURNAL OF SOLID STATE CHEMISTRY 85, 117–132 (1990)

Crystal Chemistry and Phase Equilibria Studies of the $BaO(BaCO_3)$–R_2O_3–CuO Systems. IV. Crystal Chemistry and Subsolidus Phase Relationship Studies of the CuO-Rich Region of the Ternary Diagrams, R = Lanthanides

WINNIE WONG-NG, BORIS PARETZKIN, AND EDWIN R. FULLER, JR.

Ceramics Division, IMSE, National Institute of Standards and Technology, Gaithersburg, Maryland 20899

Received August 16, 1989; in revised form November 20, 1989

In the $BaO(BaCO_3)$–R_2O_3–CuO systems, where R = lanthanides and yttrium, general trends of phase formation, solid solution formation, and phase relationships are correlated with the ionic size of R. In air at 950°C the phase relationships in the CuO-rich region of these ternary diagrams progressively change from the La system through the Nd, Sm, Eu, Gd, Y, Ho systems to the Er system. First, the La system has the greatest number of ternary compounds. Second, the superconductor material, $Ba_2RCu_3O_{6+x}$, exhibits a solid solution of $Ba_{2-z}R_{1+z}Cu_3O_{6+x}$ for the first half of the lanthanide elements with a range of formation which varies with the ionic size of R. Third, a trend is observed regarding the tie-line connections between BaR_2CuO_5, CuO, the phases $Ba_{2-z}R_{1+z}Cu_3O_{6+x}$, and the binary phase R_2CuO_4 or $R_2Cu_2O_5$. For the first half of the lanthanides, except for La, a compatibility join is found to connect R_2CuO_4 and the tetragonal end member of the $Ba_{2-z}R_{1+z}Cu_3O_{6+x}$ phase. In systems where R has a smaller ionic size, R = Eu and beyond, the tie-line connection switches to join the BaR_2CuO_5 phase and the CuO phase. For R = Dy and beyond, the binary phase R_2CuO_4 is replaced by the binary phase $R_2Cu_2O_5$. © 1990 Academic Press, Inc.

Introduction

Despite recent worldwide efforts in superconductivity research, a lack of thorough fundamental understanding of the Ba–Y–Cu–O systems still remains. In addition, problems such as low critical current density, flux creep, and poor mechanical properties still render practical applications of these materials as a great challenge. The discovery that substitution of most lanthanide elements, R, for Y also produces a superconductor with a transition temperature ≈90 K (*1*, *30*) provides numerous alternative materials for investigations of possible desirable properties.

Since knowledge of phase equilibria and crystal chemistry is essential for controlling processing parameters and understanding material properties, systematic studies of the Ba–R–Cu–O systems are crucial. As part of an ongoing effort to understand the crystal chemistry and phase equilibria of the $BaO(BaCO_3)$–R_2O_3–CuO systems (*2*–*9*), we have initiated a systematic investigation of trends in phase formation and solid solution formation of selected binary and ternary compounds in the $BaO(BaCO_3)$–

0022-4596/90 $3.00
Copyright © 1990 by Academic Press, Inc.
All rights of reproduction in any form reserved.

R_2O_3–CuO systems and trends in structural phase transformation between the orthorhombic and tetragonal phases of the superconductor material, $Ba_2RCu_3O_{6+x}$, as a function of the ionic size of the element R.

Solid solution formation for a material is also of technological importance. For example, one may control and correlate properties and processing parameters by varying the composition of the materials. In a recent study correlating superconducting properties with solid solution formation in the series $Ba_{2-z}R_{1+z}Cu_3O_{6+x}$, where R = Nd, Sm, Eu, and Gd, Blendell *et al.* (*9*) observed that the amount of substitution of a lanthanide for barium decreases regularly with the decreasing size of R^{3+}: the larger the mismatch of the ionic size between R^{3+} and Ba^{2+}, the narrower the extent of solid solution. The solid solution formation terminates at Gd, which seems to separate the different behavior of the earlier and later lanthanide elements. Recently, we have investigated the $Ba_{2-z}Sm_{1+z}Cu_3O_{6+x}$ and the $Ba_{2-z}La_{1+z}Cu_3O_{6+x}$ series and are able to establish a more general trend of solid solution formation. Current results are described herein.

Although solid solution members of the

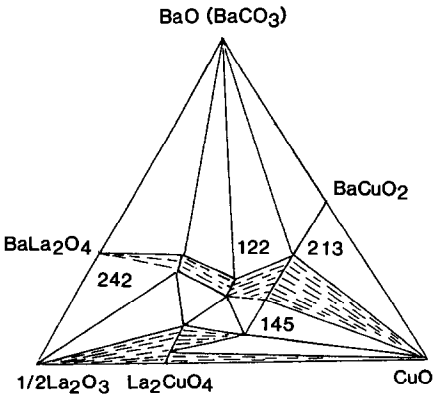

FIG. 1. Subsolidus phase diagram for the Ba–La–Cu–O system at 950°C in air, after Kilbanow *et al.* (*13*).

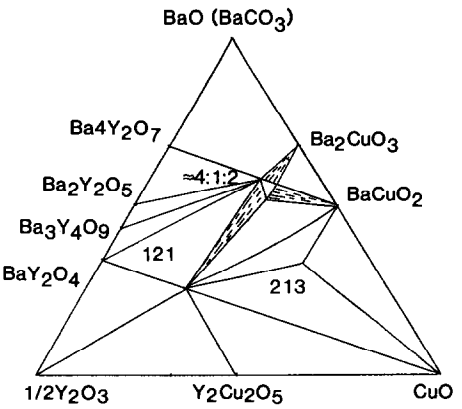

FIG. 2. Subsolidus phase diagram for the Ba–Y–Cu–O system at 950°C in air, after Roth *et al.* (*14*).

$Ba_{2-z}La_{1+z}Cu_3O_{6+x}$ system have been characterized by neutron diffraction by David *et al.* (*10*), Segré *et al.* (*11*), and Sunshine *et al.* (*12*), the solid solution range was not conclusively determined by these investigators and was assigned to be $z \lesssim 0.5$. Our studies of the solid solution formation of $Ba_{2-z}R_{1+z}Cu_3O_{6+x}$, where R = Nd, Eu, and Gd (*9*) indicated that the range of solid solution of the Nd system extends to $z \leq 0.7$. As the sizes of La^{3+} and Ba^{2+} are closer to each other than those of Nd^{3+} and Ba^{2+}, we expect the extent of solid solution in the La system to be greater or comparable to that of the Nd system. Accordingly, the range of solid solution of the $Ba_{2-z}La_{1+z}Cu_3O_{6+x}$ system was reinvestigated in the present work.

Ternary phase diagram studies of the Ba–La–Cu–O and Ba–Y–Cu–O systems at 950°C in air have been conducted by Kilbanow *et al.* (*13*) and Roth *et al.* (*14*), which are shown in Figs. 1 and 2, respectively. (Figure 1 has been modified to include present results.) Phase compatibility relationships are found to be substantially different for these two systems. The large difference in size of the La^{3+} and Y^{3+} ions undoubtedly has a great impact on their

crystal chemistry. Part of the goal of this study is to characterize and compare features of phase formation and phase relationships of compounds in the ternary phase diagrams of the $BaO(BACO_3)$–R_2O_3–CuO systems near the CuO corner.

Experimental

Solid state reaction techniques were employed for all sample preparation. Similar heat treatment procedures were adopted for all series of $Ba_{2-z}R_{1+z}Cu_3O_{6+x}$ materials. Table I shows the compositions prepared for the several solid solution series which we have investigated. Most compositions were prepared from stoichiometric mixtures of CuO, R_2O_3, and $BaCO_3$. In the case of R = La, $La(OH)_3$ was used instead of La_2O_3. Before each firing and annealing, the powder was pressed into pellets and placed on MgO single crystals, which were then set on a silica brick. The pellets were heat treated at both 850 and 900°C for 1 day, then fired in air at 950°C. Air-quenching was performed by removing the sample and brick together from the furnace and placing them on the bench top. Cooling time to room temperature for the sample was estimated to be about 3 to 5 min. Several regrindings and annealings took place until a single phase material was confirmed by the X-ray powder diffraction.

To study phase relationships in the vicinity of the superconductor solid solution, $Ba_{2-z}R_{1+z}Cu_3O_{6+x}$, and the "green phase" compound, BaR_2CuO_5, compositions near the CuO corner of selected $BaO(BaCO_3)$–R_2O_3–CuO systems were also prepared. These compositions are indicated in Table II for the La, Pr, Nd, Sm, Eu, Gd, and Er systems. The Nd system was studied in more detail and will be reported separately (*4*). Most final sinterings were performed at 950°C and air-quenched. For compositions very close to the CuO corners, a temperature of 920°C was used instead to avoid melting. Tie-line relations were established by X-ray powder diffraction characterization.

TABLE I

COMPOSITION, "z," OF SAMPLES $Ba_{2-z}R_{1+z}Cu_3O_{6+x}$ PREPARED AT 950°C IN AIR

R	z
La	0.0, 0.1, 0.2, 0.3, 0.4, 0.5, 0.6, 0.7, 0.8, 0.9, 1.0
Nd	0.0, 0.1, 0.2, 0.3, 0.4, 0.5, 0.6, 0.7, 0.8, 0.9, 1.0
Sm	0.0, 0.1, 0.2, 0.3, 0.4, 0.5, 0.6, 0.7, 0.8, 0.9, 1.0
Eu	−0.1, 0.0, 0.1, 0.2, 0.3, 0.4, 0.5, 0.6, 0.7, 0.8, 0.9, 1.0
Gd	0.0, 0.1, 0.2, 0.3, 0.5
Dy	0.0, 0.1, 0.2, 0.5
Y	0.0, 0.1, 0.5
Er	−0.1, 0.0, 0.1, 0.5
Lu	0.5

TABLE II

COMPOSITIONS NEAR THE CuO CORNERS PREPARED FOR THE TERNARY PHASE DIAGRAMS, $BaO:\frac{1}{2}R_2O_3$:CuO, IN AIR

R	Compositions $BaO:\frac{1}{2}R_2O_3:CuO$
La	10:40:50, 20:40:40
Pr	10:40:50, 20:40:40
Nd	10:60:30, 15:50:35, 10:40:50, 15:15:70, 20:10:70, 20:10:70, 25:15:60, 25:40:35, 27:33:40, 30:30:40, 35:25:40, 18:37:45, 58:08:34, 53:13:34, 21:35:44, 25:28:47, 20:40:40
Sm	25:15:60, 15:15:70, 30:30:40, 10:60:30, 25:28:47, 28:25:47, 32:20:48, 10:40:50, 20:40:40
Eu	25:15:60, 15:15:70, 30:30:40, 10:60:30, 25:28:47, 28:25:47, 32:20:48, 10:40:50
Gd	30:30:40, 10:60:30, 25:15:60, 30:25:45, 10:40:50, 32:20:48, 34:18:48
Er	32:20:48, 10:50:40, 10:40:50, 15:30:55, 20:10:70, 25:25:50, 30:30:40, 35:30:35

Results and Discussion

Results of the ternary phase compatibility diagrams of the systems $BaO(BaCO_3)$–R_2O_3–CuO in the vicinity of the CuO corners, where R = La, Nd, Sm, Eu, Gd, Y, and Er are shown in Fig. 3. Since exact tie-line connection would require detailed lattice parameter determination, the tie lines connecting the solid solution series in this report are schematic only. Proceeding from the La system, which has the largest ionic size of R, toward the Er system with a smaller ionic size, a general trend of phase formation, solid solution formation, and phase relationship is found to be correlated with the ionic size of R. Several features of the progressive changes in the appearance of these ternary diagrams near the CuO corner will be discussed in detail below. In brief, these features are (1) the La system has the largest number of ternary compounds and solid solution series; this number decreases as the size of R decreases. (Although it has been reported by de Leeuw *et al.* (*15*) that if BaO_2 or $Ba(NO_3)_2$ are used other phases such as $Ba_4YCu_3O_{8.5}$ and $Ba_8Y_3Cu_5O_{1.5}$ also form, these phases have not been confirmed in this laboratory.) (2) The superconductor material, $Ba_2RCu_3O_{6+x}$, for the first half of the lanthanide elements, i.e., R = La, Nd, Sm, Eu, and Gd, which are relatively larger in size, exhibit a solid solution of $Ba_{2-z}R_{1+z}Cu_3O_{6+x}$ with a range of formation which decreases as the size of R decreases; this solid solution region terminates at Dy and beyond, where presumably the superconductor phase assumes a point stoichiometry; (3) A trend is observed regarding the tie-line connections between BaR_2CuO_5, CuO, the superconductor phases $Ba_{2-z}R_{1+z}Cu_3O_{6+x}$, and the binary phase R_2CuO_4, or $R_2Cu_2O_5$; note that the binary phase R_2CuO_4 is replaced by the binary phase $R_2Cu_2O_5$ after the tie-line connection changes.

Current results of phase formation for several series of compounds and solid solutions in the $BaO(BaCO_3)$–R_2O_3–CuO systems are discussed individually in the sections below. Following this, features of the tie-line relationship of the four phases near the CuO corner are discussed. Crystal stuctures for some of these phases are also discussed.

I. Phase Formation near CuO Corner

1. BaR_2CuO_5 and $Ba_{2+2x}R_{4-2x}Cu_{2-x}O_{10-2x}$ (1:2:1), R = La, Nd

Details of the phase formation of the 1:2:1 phases have been reported elsewhere (*5, 6, 16, 17*). In brief, under ambient conditions, the commonly known "green phase", or BaR_2CuO_5, has been prepared for R = Sm, Eu, Gd, Dy, Y, Er, Tm, Yb, and Lu. Among the oxides with a stable R^{3+} valence state, there is a size range of R for which this phase forms. However, this phase does not form with lanthanides of larger ionic size. For example, the formation of green phases for $R = La^{3+}$ and Nd^{3+} does not take place. The materials formed in this case are brown and are found to have a completely different crystal structure from that of the "green phase". While all green phase materials are orthorhombic with space group *Pbnm*(62), Z = 4, the "brown phases" tend to form solid solutions of $Ba_{2+2x}R_{4-2x}Cu_{2-x}O_{10-2x}$, with a tetragonal space group of *P*4/*mbm*(127). The solid solution range is $0.15 \leq x \leq 0.25$ for the La system and $0.0 \leq x \leq 0.1$ for the Nd system. Note that the La solid solution series does not include the stoichiometric compound with $x = 0$.

In the green phase structure, each yttrium ion is surrounded by seven oxygen atoms, as shown in Fig. 4. The framework can be considered as built up from distorted monocapped trigonal prisms, RO_7, which share one triangular face forming R_2O_{11} blocks. There is an apparent size limit, bounded by Sm, beyond which stability of

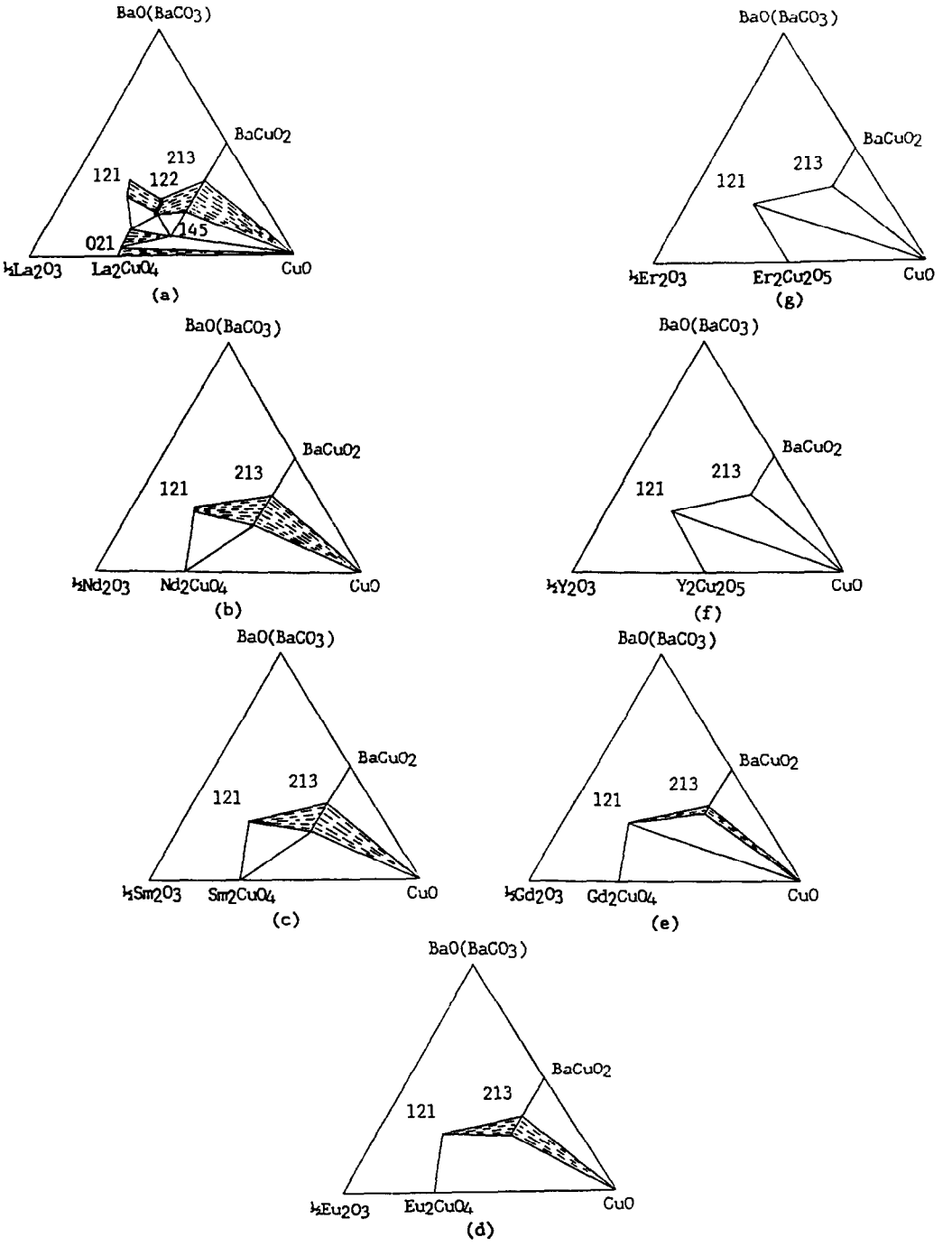

FIG. 3. Subsolidus phase compatibility diagrams of BaO–$\frac{1}{2}R_2O_3$–CuO near the CuO-rich region at 950°C in air for (a) La, (b) Nd, (c) Sm, (d) Eu, (e) Gd, (f) Y, and (g) Er.

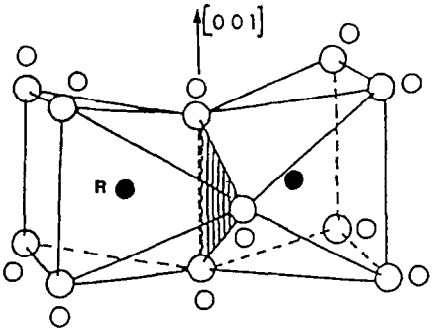

FIG. 4. Polyhedral environment of RO_7 and R_2O_{11} found in the structure of BaR_2CuO_5, R = Sm, Eu, Gd, Dy, Y, Ho, Er, Tm, Yb, and Lu.

the distorted monocapped trigonal prism, RO_7, is unattainable. The framework of the La and Nd materials is principally built from edge- and face-sharing RO_{10} and RO_8 polyhedra as illustrated in Figs. 5a and 5b. These octahedra and decahedra provide large enough space to accommodate the La^{3+} and Nd^{3+} ions.

2. $Ba_{2-z}R_{1+z}Cu_3O_{6+x}$ (2:1:3), R = La, Pr, Nd, Sm, Eu, and Gd

Results of the solid solution investigation of the R = La series show that the solid solution range indeed extends beyond z = 0.5. In Fig. 6, X-ray diffraction patterns of the $Ba_{2-z}La_{1+z}Cu_3O_{6+x}$ compositions with z = 0.5 to 0.9 are shown. A small number of peaks corresponding to $BaLa_4Cu_5O_{13+x}$ start to appear at $z \approx 0.8$. Figure 7 shows the X-ray powder diffraction patterns for selected compositions of $Ba_{2-z}Eu_{1+z}Cu_3O_{6+x}$, indicating a solid solution range of $z \leq 0.5$. The solid solution range is different for each of these series. The upper limit of the solid solution series is discernible by the presence of X-ray diffraction peaks from a different phase. For example, in the region around 2θ of 28–29° one detects the presence of the green phase BaR_2CuO_5 and CuO when R = Eu, Gd, and Er. The Sm samples show a solid solution range for $z \leq$ 0.7. The Gd sample, on the other hand, shows only a small range of $z \leq 0.2$. Solid solution ceases to exist at Dy, Er, and Y, or at least is less than $z \approx 0.1$, and this is so presumably also for superconductors with smaller R. The tendency of the solid solution formation is very great in the La system and the point compound $Ba_2LaCu_3O_{6+x}$ does not form; the lower limit of the solid solution is bounded by approximately $z >$ 0.1.

The size compatibility between the Ba^{2+} and R^{3+} is a predominant factor governing the formation of this solid solution. Shannon's ionic radii of lanthanides R^{3+}, where R = La, Pr, Nd, Sm, Eu, Gd, Dy, Y, and Er, using the coordination number of nine are listed in Tables III, IV, and V. Y is inserted according to its ionic size. The ionic radius of Ba^{2+} with a similar coordination environment is 0.147 nm, which is most comparable to that of La^{3+} of 0.122 nm. As the mismatch between R^{3+} and Ba^{2+} increases, the range of substitution decreases. Table III summarizes the approximate upper limit of the solid solution range of $Ba_{2-z}R_{1+z}Cu_3O_{6+x}$.

Another feature observed in all the $Ba_{2-z}R_{1+z}Cu_3O_{6+x}$ series is the structural phase transformation from an orthorhombic to a tetragonal structure as the value of

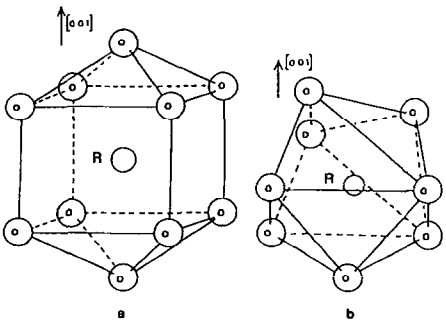

FIG. 5. Polyhedral environment of (a) RO_{10} and (b) RO_8 found in the structure of $Ba_{2+2x}R_{4-2x}Cu_{2-x}O_{10-2x}$, R = La and Nd.

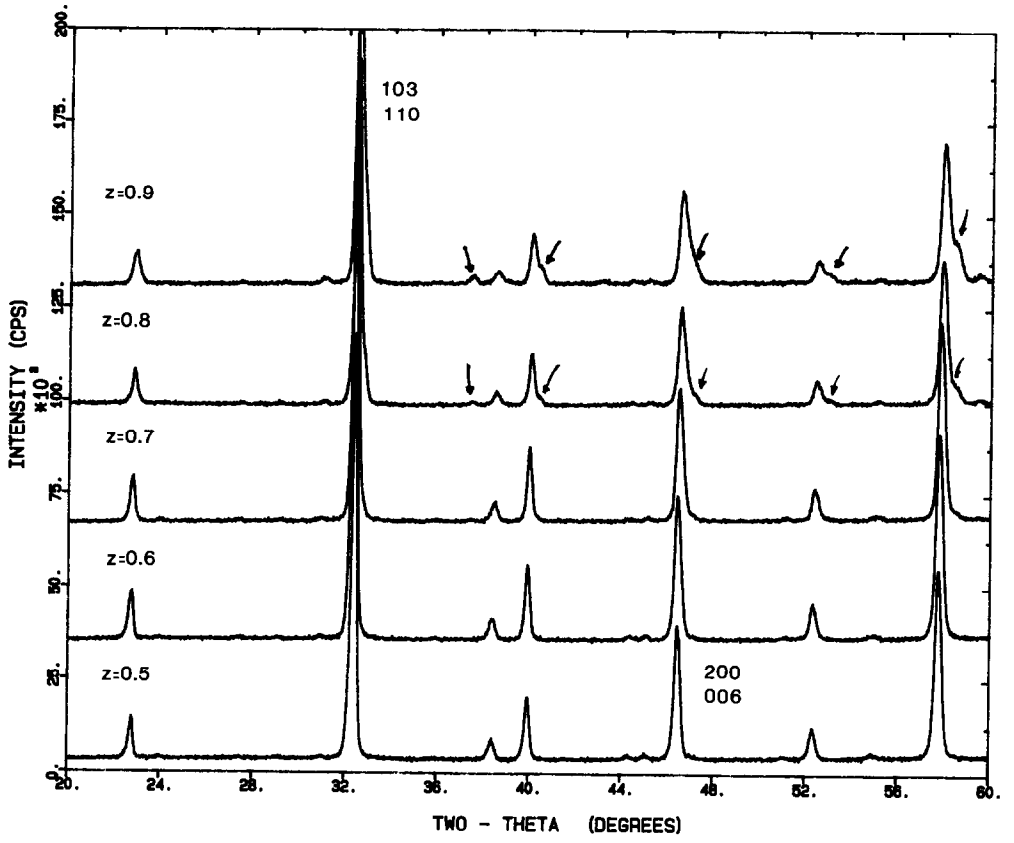

FIG. 6. X-ray diffraction patterns of $Ba_{2-z}La_{1+z}Cu_3O_{6+x}$. The appearance of the $BaLa_4Cu_5O_{13+x}$ phase is indicated by the arrows for z = 0.8 and 0.9.

z increases. Since the high temperature (950°C) phase is most likely the tetragonal structure (at least this is the case for R = Sm and Gd with z = 0 (*2, 3, 7*)), this transformation can depend on how the quenching is performed. Results discussed below only pertain to samples that were prepared at 950°C in air and air-quenched by pulling them from the furnace. The X-ray diffraction patterns of $Ba_{2-z}Eu_{1+z}Cu_3O_{6+x}$ shown in Fig. 7 illustrate the progressive changes of peak shape and convergence of multiplets into singlets going from the orthorhombic to the tetragonal structure. Phase transformation of the $Ba_{2-z}La_{1-z}Cu_3O_{6+x}$ series has been reported to take place at a z value of 0.15 (*12*). Our X-ray diffraction patterns are consistent with this result, showing a phase transformation at a z value between 0.1 and 0.2. For the Nd,

TABLE III

SOLID SOLUTION EXTENT OF $Ba_{2-z}R_{1+z}Cu_3O_{6+x}$

R	z	Ionic radius (nm)
La	≤ 0.7	0.1216
Nd	≤ 0.7	0.1163
Sm	≤ 0.7	0.1132
Eu	≤ 0.5	0.1120
Gd	≤ 0.2	0.1107

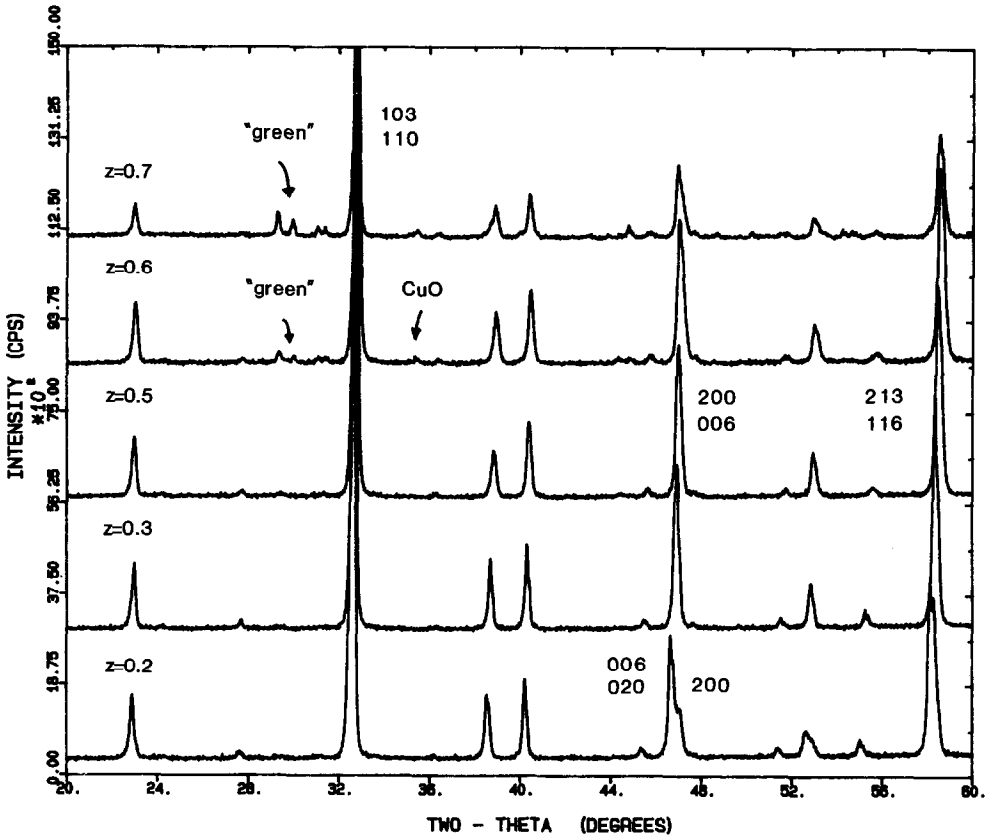

FIG. 7. X-ray diffraction patterns of $Ba_{2-z}Eu_{1+z}Cu_3O_{6+x}$.

Sm, and Eu series the corresponding z values for the structural phase transformation are approximately the same; all found to be between $z = 0.2$ and 0.3. As the samples in each $Ba_{2-z}R_{1+z}Cu_3O_{6+x}$ series were prepared at intervals in z of 0.1, we are not able to distinguish any differences at this stage. Whether the z value varies as a function of the size of R is a subject of interest to be investigated in the near future.

X-ray characterization and X-ray powder standard diffraction patterns of the tetragonal $Ba_{1.5}R_{1.5}Cu_3O_{7+x}$, with R = La, Pr, Nd, Sm, and Eu composition, has been reported (*8*). These tetragonal phases have up to 25% substitution of R in the Ba sites and therefore the chemical formula can be represented as $(Ba_{0.75}R_{0.25})_2RCu_3O_{7+x}$, or simply referred to as the $Ba_3R_3Cu_6O_{14+x}$ (336) composition. The crystallographic relationship of these five materials can be described as $a = b \approx \frac{1}{3}c$, indicating that as the R^{3+} ions replace the Ba^{2+} ions to an extent of 25% the unit cell content can be considered as a stack of three pseudo-cubes. The $Ba_3La_3Cu_6O_{14+x}$ system was first studied by Provost *et al.* (*18*) and the crystal structure has been determined by Sunshine *et al.* (*12*) using the neutron powder diffraction technique. This structure is similar to the structure of the superconductor $Ba_2YCu_3O_{6+x}$ except it is tetragonal with smaller unit cell volume, and with oxygen partially located at both the *a*- and *b*-basal axes. The struc-

tures of the Pr, Nd, Sm, and Eu analogs are presumably isostructural with the La compound because of the similarity of the X-ray diffraction patterns. Neutron diffraction study of the $Ba_3Nd_3Cu_6O_{14+x}$ phase is currently underway (*19*) to confirm the structure as well as the oxygen content of this material.

The superconductivity properties of the solid solution are currently being selectively investigated in terms of the ac magnetic susceptibility and critical current density measurements. For each series of materials a general trend of T_c diminishing as the z value increases has been observed. The T_c values, the fraction of superconductivity, and the critical current density are currently being studied and will be reported separately.

3. $BaR_4Cu_5O_{13+x}$ (1 : 4 : 5)

This oxygen defect perovskite is characterized by a mixed valence of Cu(II) and Cu(III) despite the presence of numerous oxygen vacancies. The La system appears to be the only one among the lanthanide systems that forms this black metallic conductor. The $BaLa_4Cu_5O_{13+x}$ compound is tetragonal with space group $P4/m$. The lattice parameters of a sample which was prepared in air at 950°C was found to have lattice parameters a = 0.86602(5) nm and c = 0.38629(3) nm (*20*) at approximately 25°C, which are closely related to that of the cubic perovskite: $a \approx a_p \sqrt{5}$ and $c = a_p$ = 3.8594. Michel *et al.* (*21*) described the framework $[Cu_5O_{13}]$ to be built up from corner-sharing CuO_5 pyramids and CuO_6 octahedra forming hexagonal tunnels and perovskite cages where the La^{3+} and Ba^{2+} ions are located in an ordered manner. Figure 8 (*22*) shows the structure of $BaLa_4Cu_5O_{13}$ in which each CuO octahedron shares four corners with four pyramids, and the two remaining corners with two other octahedra. Each pyramid is then connected to four other pyramids and one octahedron. Oxygen vacancies, which are found to be between pairs of CuO_5, form one-dimensional channels along the z-axis. The lanthanum ions are located in the hexagonal tunnels whereas the barium ions are located in the perovskite tunnels.

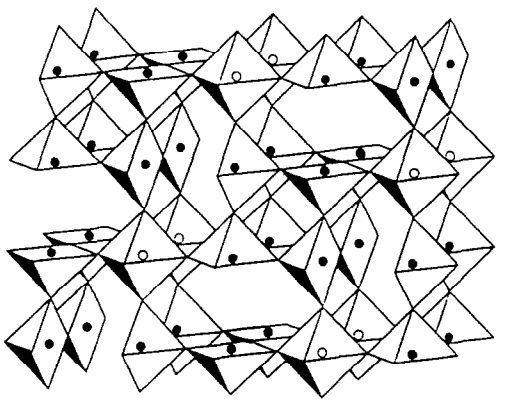

FIG. 8. Crystal structure of the compound $BaLa_4Cu_5O_{13}$ (*18*). The solid and open circles represent Cu atoms belonging to the CuO_5 pyramids and the CuO_6 octahedra, respectively. La^{3+} and Ba^{2+} ions are located in the hexagonal and perovskite tunnels, respectively. The z-axis points out of the plane of the paper.

4. $Ba_{1+x}R_{2-x}Cu_2O_{6-x/2}$ (1 : 2 : 2)

Among the BaO : $\frac{1}{2}R_2O_3$: CuO systems, the black 1 : 2 : 2 phase $BaR_2Cu_2O_6$ has only been prepared successfully in the La analog. The compounds $A_{1+x}La_{2-x}Cu_2O_{6-x/2}$ were first isolated by Nguyen *et al.* (*23*) with $0 \le x \le 0.14$ for A = Sr and x = 0.10 for A = Ca. These compounds are reported to be tetragonal with $a \approx 0.390$ nm and $c \approx 2.0$ nm and with a space group of $I4/mmm$. The structure, which is derived from that of $Sr_3Ti_2O_7$, can be described as an intergrowth of "oxygen-deficient, double-perovskite" layers and of SrO-type layers. These perovskite layers are indicated in Fig. 9. When A = Ba, the extent of solid solution has been found to be $0 \le x \le 0.20$ by Kilbanow *et al.* (*13*). X-ray diffraction studies and lattice parameter determination

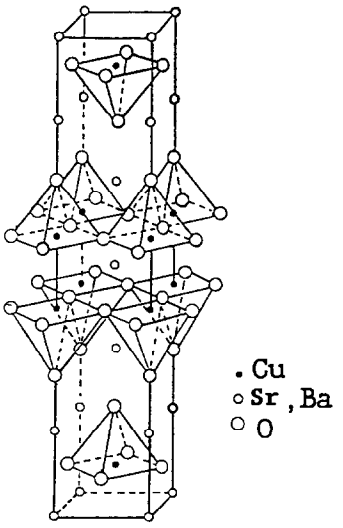

FIG. 9. Crystal structure of the compound $Sr_2La_4Cu_4O_{12}$ showing the oxygen-deficient double perovskite layers (Nguyen *et al.* (*19*)).

for the solid solution series $Ba_{1+x}La_{2-x}Cu_2O_{6-x/2}$ is currently being conducted.

5. R_2CuO_4 (0:2:1)

While all the R_2O_3:CuO systems contain only one binary compound at ambient atmosphere, there exist two distinctive compositions. Binary compounds of 2:1 composition with general formula R_2CuO_4 can be prepared with the lighter and larger size of R, for example with R = La, Pr, Nd, Sm, Eu, and Gd, whereas oxides in the second half of the lanthanide series tend to form a $2(\frac{1}{2}R_2O_3):2CuO$ binary compound $R_2Cu_2O_5$. Not all R_2CuO_4 phases are isostructural. For example, while La_2CuO_4 is orthorhombic with space group *CmCa* (*24*) and has the distorted K_2NiF_4-type structure as shown in Fig. 10, Pr_2CuO_4, Nd_2CuO_4, Sm_2CuO_4, Eu_2CuO_4, and Gd_2CuO_4 are tetragonal with space group *I4/mmm*. These tetragonal structures do not resemble the K_2NiF_4 type but have a coplanar Cu–O layer similar to that found in CaF_2-type structure (*25*). These features are illustrated in Fig. 10. Doping the La_2CuO_4 structure with a small amount of a 2+ ion such as Ba^{2+} and Sr^{2+} changes the structure from orthorhombic to tetragonal (*26, 27*) and results in a superconductor phase. Typical X-ray patterns of the orthorhombic and tetragonal R_2CuO_4 are illustrated with La_2CuO_4 and Nd_2CuO_4 in Fig. 11. Substantial differences of these patterns arising from totally different structures are obvious.

Solid solution formation of the composi-

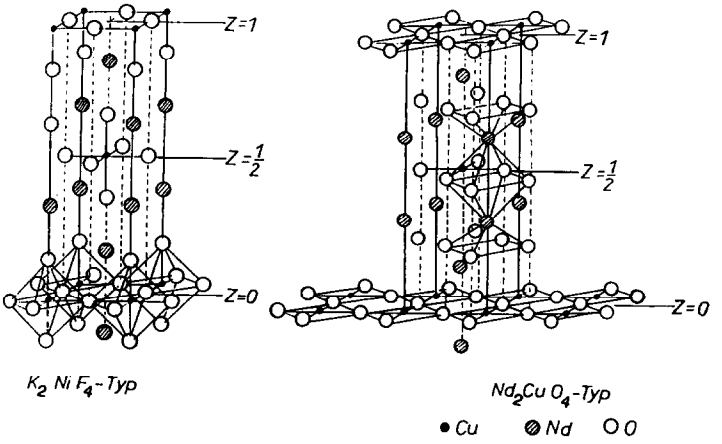

FIG. 10. Crystal structures of R_2CuO_4 for (a) R = La and (b) R = Pr, Nd, Sm, Eu, and Gd.

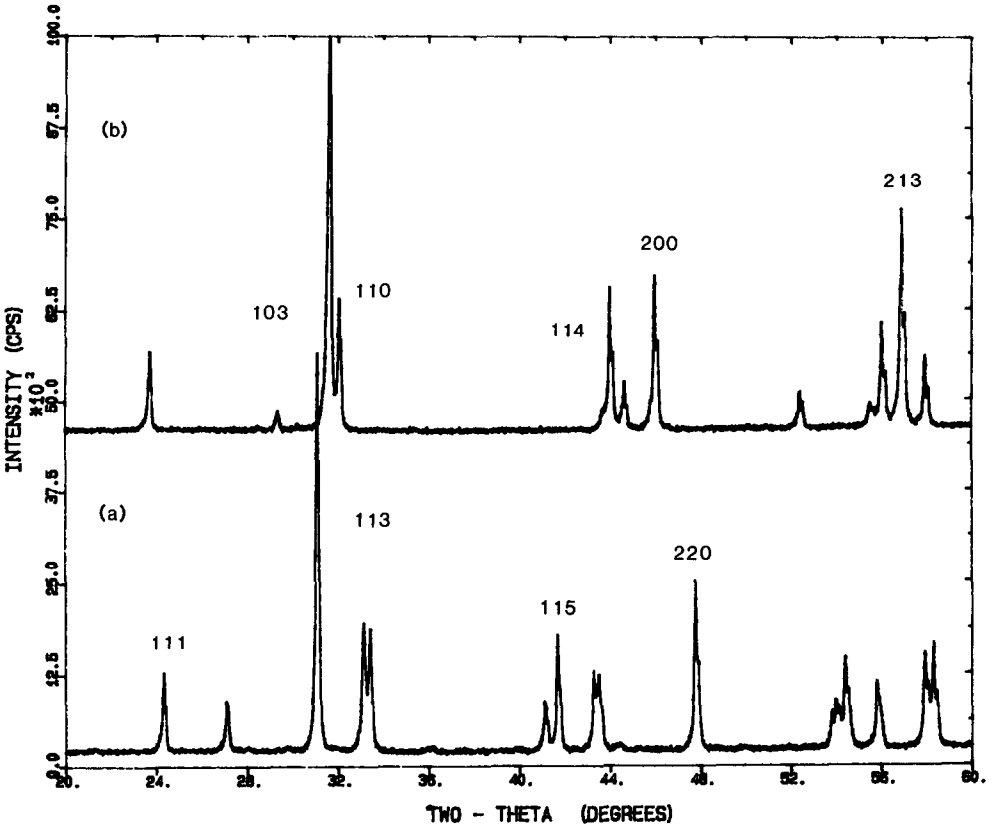

FIG. 11. X-ray diffraction patterns of (a) La_2CuO_4 and (b) Nd_2CuO_4.

tions $(R_{2-x}A_x)CuO_4$ with A = Ba has been studied with R = La (*12*) and that with a solid solution range of $0 \leq x \leq 0.25$ has been reported. This series gives rise to superconductor materials of T_c around 30 K (*28*). Substitution of Nd^{3+} and other smaller R^{3+} by Ba^{2+} in the R_2CuO_4 phases cannot be prepared (with $x \geq 0.1$).

Since crystallographic data are essential for phase characterization, Table IV summarizes these data and the corresponding Powder Diffraction File Number (PDF No.) (*29*) for the binary R_2CuO_4 phases which have been reported in the literature and from this work. The crystallographic data for the "green" and "brown" phases and the high T_c superconductor phases have been reported elsewhere (*5, 29–31*). Figure 12 illustrates a plot of the cell volume V of R_2CuO_4 versus the ionic radii of Shannon. The monotonic decrease in crystallographic volumes, as the ionic radii of the lanthanides decrease across the series, follows the well-known lanthanide contraction. The deviation from this linear dependence of the Gd compound may be due to the special stability associated with the half-filled Gd^{3+} ($4f^7$) f-subshell.

6. $R_2Cu_2O_5$ (0 : 1 : 1)

$R_2Cu_2O_5$ are greenish in color and can be prepared with the second half of the lanthanides, with R = Tb, Dy, Ho, Y, Er, Tm, Yb, and Lu. Structure determinations of

TABLE IV

CRYSTALLOGRAPHIC DATA FOR R_2CuO_4

Compound R_2CuO_4	Space group	Cell parameters a, b, c (nm)	Cell volume V (nm^3)	Density (g/cm^3)	Ionic radius R (nm)	PDF No.
La_2CuO_4	*Fmmm*	0.53556(6) 0.54011(9) 1.3149(5)	0.38035	7.079	0.1216	38-709
$(Ba_{.9}La_{.1})_2CuO_4$	*I4/mmm*	0.37754(6) 1.3236(14)	0.18866	7.130	0.1216	38-1308
Pr_2CuO_4	*I4/mmm*	0.3958 1.2288	0.19250	7.062	0.1179	22-245
Nd_2CuO_4	*I4/mmm*	0.394366(12) 1.21693(5) (at ≈25°C)	0.18926	7.300	0.1163	39-1390 (*32*)
Sm_2CuO_4	*I4/mmm*	0.3905 1.1938	0.18204	7.814	0.1132	24-998
Eu_2CuO_4	*I4/mmm*	0.3895 1.1887	0.18034	7.946	0.1120	24-399
Gd_2CuO_4	*I4/mmm*	0.3889 1.1861	0.17939	8.184	0.1107	24-422

$R_2Cu_2O_5$ have been controversial in the past 25 years. In 1964, Schmitz-DuMont and Kasper (*33*) identified $R_2Cu_2O_5$, where R = Y, Dy, Er, Yb, and Tb, to be orthorhombic double oxides having $In_2Cu_2O_5$-type structure. $In_2Cu_2O_5$ was later redetermined by Bergerhoff and Kasper (*34*) to be monoclinic with space group $P2$ and cell parame-

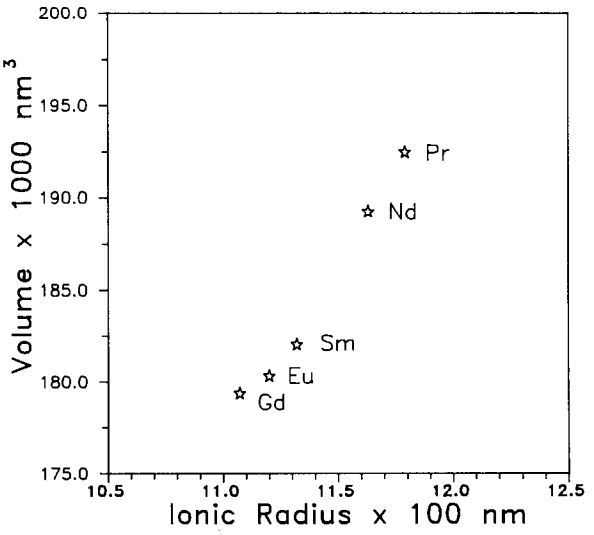

FIG. 12. Dependence of the unit cell volume of R_2CuO_4 on the ionic radius of R for R = Pr, Nd, Sm, Eu, and Gd.

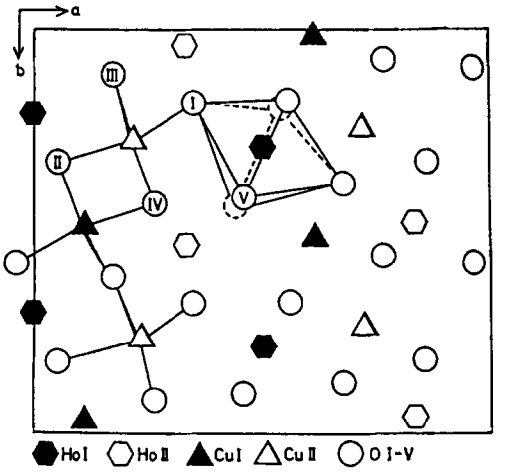

FIG. 13. Projection for $Ho_2Cu_2O_5$ along [001].

ters of a = 2.462, b = 1.0537, c = 0.3280 nm, and γ = 133°. The structure consists of a pseudo-orthorhombic framework of InO_6 polyhedra with the oxygen atoms at the corners.

In 1977, Freund and Muller-Buschbaum (*35*) reported the structure of the Ho analog, using single crystals obtained by melting the oxide mixture (2 CuO : 1 Ho_2O_3) with KF as a flux, to be orthorhombic. They found that the crystal structures of the Ho and the In compounds (*34*) are significantly different, particularly the coordination sphere around the Cu^{2+}. Figure 13 shows the atom distribution of the unit cell of $Ho_2Cu_2O_5$. Unlike those of many other oxo–cuprates, the Cu^{2+} has been found to have four nearest oxygen neighbors arranged in a distorted tetrahedron configuration. Figure 13 further shows that two each of these polyhedra share a common edge and are connected via corners in a wavelike chain along [010]. The Ho^{3+} ions are surrounded by octahedra which form one-dimensional infinite chains connected via edges.

The structures and X-ray diffraction patterns of all seven $R_2Cu_2O_5$ compounds were later reexamined by E. Lambert in 1981 and 1982 (*36*). All materials were found to be isostructural and have the $Ho_2Cu_2O_5$-type structure with space group $Pna2_1$. Table V summarizes the crystallographic data and the PDF No. for eight binary $R_2Cu_2O_5$ phases, where R = lanthanide and yttrium. Figure 14 illustrates a plot of the cell volume V, of $R_2Cu_2O_5$ versus the ionic radii of Shannon. Similar to the corresponding plot of the R_2CuO_4 compounds, a monotonic decrease in crystallographic volumes is also observed as the ionic radius of the lanthanides decreases across the series.

II. Tie-Line Relationships

After the description of the crystal chemistry of individual phases and solid solution series in the CuO-rich region of the BaO–$\frac{1}{2}R_2O_3$–CuO systems, we are in a position to discuss the trend of the ternary diagrams

TABLE V

CRYSTALLOGRAPHIC DATA FOR $R_2Cu_2O_5$

Compound $R_2Cu_2O_5$[a]	Cell parameters a, b, c (nm)	Cell volume V (nm^3)	Density (g/cm^3)	Ionic radius R (nm)	PDF No.
$Tb_2Cu_2O_5$	1.0861 0.35455 1.2535	0.48269	7.223	0.1095	34-385
$Dy_2Cu_2O_5$	1.0837 0.35194 1.2485	0.47617	7.422	0.1083	33-455
$Y_2Cu_2O_5$	1.0799 0.34960 1.2456	0.47025	5.537	0.1075	33-511
$Ho_2Cu_2O_5$	1.0806 0.34950 1.2470	0.47095	7.573	0.1072	33-458
$Er_2Cu_2O_5$	1.0776 0.34714 1.2438	0.46528	7.732	0.1062	33-456
$Tm_2Cu_2O_5$	1.0742 0.34565 1.2382	0.45974	7.873	0.1052	34-386
$Yb_2Cu_2O_5$	1.0724 0.34329 1.2349	0.45462	8.082	0.1042	33-507
$Lu_2Cu_2O_5$	1.0698 0.34102 1.2358	0.45085	8.206	0.1032	34-387

[a] All isostructural, orthorhombic with space group $Pna2_1$.

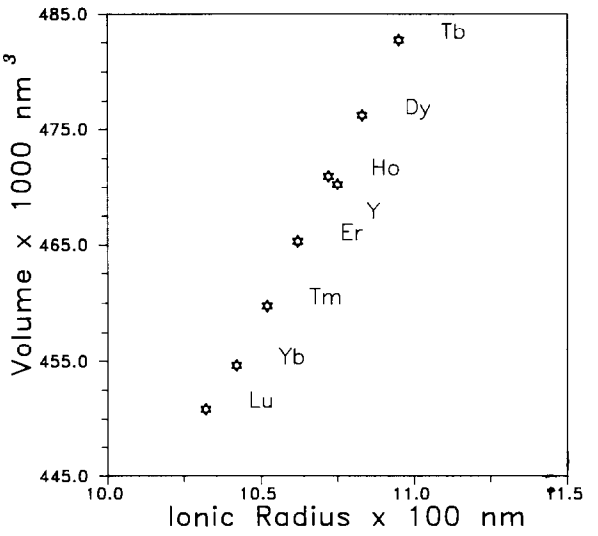

FIG. 14. Dependence of the unit cell volume of $R_2Cu_2O_5$ on the ionic radius of R for R = Tb, Dy, Y, Ho, Er, Tm, Yb, and Lu.

illustrated in Fig. 3. The La diagram appears to be the most complicated one. The presence of four solid solution series ($Ba_{2+2x}R_{4-2x}Cu_{2-x}O_{10-2x}$, $Ba_{2-z}R_{1+z}Cu_3O_{6+x}$, $Ba_{1+x}R_{2-x}Cu_2O_{6-x/2}$, and $R_{2-x}Ba_xCuO_4$) as well as the compound $BaR_4Cu_5O_{13+x}$ in the La system further makes the tie-line connection very different from the rest of the lanthanide series. The number of solid solution series changes into two in the Nd system ($Ba_{2+2x}R_{4-2x}Cu_{2-x}O_{10-2x}$, $Ba_{2-z}R_{1+z}Cu_3O_{6+x}$) and reduces into one at the Sm diagram ($Ba_{2-z}R_{1+z}Cu_3O_{6+x}$). The extent of the $Ba_{2-z}R_{1+z}Cu_3O_{6+x}$ solid solution decreases as the mismatch between Ba^{2+} and R^{3+} increases. This range of solid solution diminishes and ceases to exist beyond R = Gd. After the Gd system, only stoichiometric point compounds are found in the CuO-rich region.

Another feature of these diagrams is illustrated by the tie-line connection between the binary compound along the $\frac{1}{2}R_2O_3$–CuO edge to the 121 phase and the 213 series. As has been discussed previously, the R_2CuO_4 compound can only be prepared with the larger size of R, namely, from La to Gd, while the $R_2Cu_2O_5$ phase exists with the smaller size of R. The tie-line connection between this binary composition R_2CuO_4/$R_2Cu_2O_5$ to the 121 phase or the high T_c superconductor compositions appear to reflect the different extent of the $Ba_{2-z}R_{1+z}Cu_3O_{6+x}$ solid solution. When Rs are relatively large and the extent of the solid solution line is long, e.g., R = La, Nd, and Sm, a compatibility line is found to connect the R_2CuO_4 and the tetragonal end member of the $Ba_{2-x}R_{1+x}Cu_3O_{6+x}$ phase. In the systems with R = Eu and Gd, the tie-line connection switches to join the CuO phase and the $BaEu_2CuO_5$/$BaGd_2CuO_5$ phase, respectively. This trend remains hereafter in the systems with smaller Rs.

Conclusion

The size of the lanthanides, R^{3+}, has been found to have a profound effect on the trend of phase and solid solution formation

as well as phase compatibility relationships in the CuO-rich region of the BaO–$\frac{1}{2}R_2O_3$–CuO systems. The larger the size of R^{3+}, the greater the number of ternary compounds and solid solution series formed. In the series of $Ba_{2-z}R_{1+z}Cu_3O_{6+x}$, solid solution formation was identified to exist with the larger size rare-earth ions, namely, La, Pr, Nd, Sm, Eu, and Gd. The range of this solid solution formation decreases with increasing difference between the size of Ba^{2+} and R^{3+}. The trend of tie-line connection is also found to be dependent on the size of R^{3+}.

It is hoped that the relationships among compositions, structures, and the size of R^{3+} discussed in this report will enhance the understanding of the physical properties of high T_c superconductors and improve the strategy both for processing these materials with improved properties and for the search for new materials. Further work will continue in the phase equilibria studies of these lanthanide systems including the investigation of melting relationships and primary phase field determination of selective $Ba_2RCu_3O_{6+x}$ phases and of mixed lanthanide phases.

Acknowledgments

This project is partially supported by the Electric Power Research Institute. The valuable discussion with Drs. L. P. Cook and R. S. Roth and the critical review of the manuscript by Drs. H. F. McMurdie and S. Dapkunas are appreciated. Acknowledgment is also due to Ms. R. Drew for her performance of the ac magnetic susceptibility measurement.

References

1. Y. Le Page, T. Siegrist, S. A. Sunshine, L. F. Schneemeyer, D. W. Murphy, S. M. Zahurak, J. V. Waszczak, W. R. McKinnon, J. M. Tarascon, G. W. Hull, and L. H. Greene, *Phys. Rev. B* **36,** 3617 (1987).
2. W. Wong-Ng, L. P. Cook, C. K. Chiang, L. J. Swartzendruber, L. H. Bennett, J. E. Blendell, and D. Minor, *J. Mater. Res.* **3,** 5 (1988).
3. W. Wong-Ng, L. P. Cook, C. K. Chiang, L. J. Swartzendruber, and L. H. Bennett, *in* "Ceramic Superconductors II" (M. F. Yan, Ed.), pp. 27–42, Amer. Ceram. Soc. (1988).
4. W. Wong-Ng, M. A. Kuchinski, B. Paretzkin, J. Stalick, and E. R. Fuller, Jr., *J. Amer. Ceram. Soc.*, to be submitted for publication.
5. W. Wong-Ng, M. A. Kuchinski, H. F. McMurdie, and B. Paretzkin, *Powder Diffr.* **4**(1), 1 (1989).
6. W. Wong-Ng, and B. Paretzkin, *Powder Diffr.*, to be submitted for publication.
7. W. Wong-Ng, L. P. Cook, C. K. Chiang, M. D. Valdin, D. L. Kaiser, F. Beech, L. J. Swartzendruber, L. H. Bennett, and E. R. Fuller, Jr., submitted for publication.
8. W. Wong-Ng, B. Paretzkin, and E. R. Fuller, Jr., *Powder Diffr.*, in press.
9. J. E. Blendell, W. Wong-Ng, C. K. Chiang, R. D. Shull, and E. R. Fuller, Jr., *in* "Proceedings of the Annual Meetings of the Metallurgical Society, Las Vegas, Nevada, February 1989," in press.
10. W. I. F. David, W. T. A. Harrison, R. M. Ibberson, M. T. Weller, J. R. Grasmeder, and P. Lanchester, *Nature (London)* **328,** 328 (1987).
11. C. U. Segre, B. Dabrowski, D. G. Hinks, K. Zhang, J. D. Jorgensen, M. A. Beno, and I. K. Schuller, *Nature (London)* **329,** 227 (1987).
12. S. A. Sunshine, L. F. Schneemeyer, J. V. Waszczak, D. W. Murphy, S. Miraglia, A. Santoro, and F. Beech, *J. Cryst. Growth* **85**(4), 632 (1987).
13. D. Kilbanow, K. Sujata, and T. O. Mason, *J. Amer. Ceram. Soc.* **71**(5), C267 (1988).
14. R. S. Roth, C. J. Rawn, F. Beech, J. D. Whitler, and J. O. Anderson, *in* "Ceramic Superconductors II" (M. F. Yan, Ed.), pp. 13–26 Amer. Ceram. Soc. (1988).
15. D. M. de Leeuw, C. A. H. A. Mutsaers, C. Langereis, H. C. A. Smoorenburg, and P. J. Rommers, *Physica C,* **152,** 39 (1988).
16. C. Michel, L. Er-Rakho, and B. Raveau, *J. Solid State Chem.* **39,** 161 (1981).
17. C. Michel and B. Raveau, *J. Solid State Chem.* **43,** 73 (1982).
18. T. Provost, F. Struder, C. Michel, and B. Raven, *Synth. Met.* **4,** 147 (1981).
19. J. Stalick and W. Wong-Ng, in preparation.
20. W. Wong-Ng, M. A. Kuchinski, H. F. McMurdie, and B. Paretzkin, *Powder Diffr.* **4**(1), 46 (1989).
21. C. Michel, L. Er-Rakho, M. Hervieu, J. Pannetier, and B. Raveau, *J. Solid State Chem.* **68,** 143 (1987).
22. F. Herman, *Phys. Rev. B* **37,** 2309 (1988).

23. N. NGUYEN, L. ER-RAKHO, C. MICHEL, J. CHORSNET, AND B. RAVEAU, *Mater. Res. Bull.* **15,** 891 (1980).
24. B. GRANDE, HK. MULLER-BUSCHBAUM, AND M. SCHWEIZER, *Z. Anorg. Allg. Chem.* **428,** 120 (1977).
25. HK. MULLER-BUSCHBAUM AND W. WOLLSCHLAGER, *Z. Anorg. Allg. Chem.* **414,** 76 (1975).
26. A. SANTOROR, *in* "High Temperature Superconductivity" (J. W. Lynn, Ed.), Chap. 4, Vol. 84, Springer-Verlag, New York/Berlin, to be published.
27. J. D. JORGENSEN, H.-B. SCHUTTLER, D. G. HINKS, D. W. CAPONE II, K. ZHANG, AND M. B. BRODSKY, *Phys. Rev. Lett.* **58**(10), 1024 (1989).
28. J. G. BEDNORZ AND K. A. MÜLLER, *Z. Phys. B: Condens. Matter* **64,** 189 (1986).
29. Powder Diffraction File (PDF), JCPDS-International Center of Diffraction Data, Swarthmore, PA 19081.
30. T. J. KISTENMACHER, *Solid State Commun.* **65**(9), 981 (1988).
31. W. WONG-NG, H. F. MCMURDIE, B. PARETZKIN, M. A. KUCHINSKI, AND A. L. DRAGOO, *Powd. Diff.* **2**(3), 191 (1987); **2**(4), 257 (1987); **3**(1), 47 (1988); **3**(2), 113 (1988); **3**(3), 179 (1988); **3**(4), 246 (1988); **4**(1), 40 (1989); **4**(2), 106 (1989).
32. W. WONG-NG, H. F. MCMURDIE, B. PARETZKIN, M. A. KUCHINSKI, AND A. L. DRAGOO, *Powd. Diff.* **4**(2), 106 (1989).
33. O. SCHMITZ-DUMONT AND H. KASPER, *Monatsh. Chem.* **96,** 506 (1965).
34. G. BERGERHOFF AND H. KASPER, *Acta Crystallogr. B* **24,** 388 (1968).
35. H.-R. FREUND AND HK. MULLER-BUSCHBAUM, *Z. Naturforsch., B* **32,** 609 (1977).
36. E. LAMBERT, JCPDS Grant-in-Aid Report (1981) and (1982).